THE CRATER DISTRIBUTION IN THE LOW LATITUDE REGIONS OF PHOBOS. I. Kajitani[1], H. Kikuchi[1], [1]ISAS, JAXA (kajitani.iori@jaxa.jp)

Introduction: Phobos, one of the two moons of Mars, has characteristic geological features in the lower latitude, for example, blue unit, Stickney crater, and grooves. The blue unit is a region with high albedo and a relatively flatter spectral slope than others [1]. Stickney crater is the largest crater on Phobos, with a diameter of ~9 km [2]. Grooves are long linear depression in a regolith, typically have 100–200 m wide, 10–20 m deep [3]. Those are interpreted to be features that are related to generating craters. In addition, the low latitude regions of Phobos are planned to be sampled by JAXA's Martian Moons eXploration (MMX). The MMX spacecraft is scheduled for launch in 2024. To determine where the MMX should land, it is useful to investigate what crater density distribution is observed in each region using the image data available now. Thus, our study aims to investigate the crater distributions in low-latitude regions where these geological features are observed.

Previous study manually counted craters, though not globally, using images acquired by Viking orbiter images [4]. Other study using Mars Global Surveyor data looked specifically at craters around Stickney crater in detail [5]. A global crater catalog was created by applying a crater detection algorithm to recent data from Mars Express [6].

In this study, we conducted manually crater countering in the lower latitude (±30 degree) by putting high resolution images on the recent three-dimensional model [7] and create a correct database of the location and radius of craters. In addition, we compared between some regions which was divided in equal latitude and longitude.

Method: The surface in lower latitude was classified into 4 categories (Figure1): Mars side (on the side facing Mars), anti-Mars side (on the side facing away from Mars), leading side (on the side of Phobos' progress), and tracking side (on the side opposite to Phobos' progress). We counted craters for each of the 8 regions between 30 °N and 30 °S every 30 ° longitude. For crater counting, the following resources were utilized. 8 images captured by the Viking orbiters; 77 images captured by Super Resolution Channel onboard Mars Express. The resolutions of these images are 4.4–36.8 m/pixel. The Small Body Mapping Tool [7] was used to measure the diameters and locations of craters for this study. Then, we made figures of size-frequency distribution (SFD) of Phobos's craters based on the crater list by using Craterstats [8].

Results: The results of the crater counting are shown in Table 1. The areas of the regions where craters were counted in this study range from 67.2–89.6 km^2, and the maximum and minimum crater diameters are 3.7 km and 0.011 km, respectively. Figure 2 show the cumulative crater SFDs compared in the 4 areas. The absolute values of the powers of the crater cumulative SFDs tend to be higher than previously reported results for many of the regions [9]. For the tracking side, it tended to be relatively low. The power law index of tracking side is expected to be statistically low because the number of images is small, and the resolution is low.

Discussion:

Size-frequency distribution. Considering the resolution of the images used, we treat craters larger than 200 m as relatively reliable data. It is difficult to estimate surface ages from crater counting because all areas have reached near saturation. Comparing the cumulative crater SFD in Figure 2 with the global average (data is from a crater catalog of PH9224GT) of previous studies [9], we find that overall, the crater density is greater in the 100–300 m range of crater diameters. When focusing on the same range of crater diameters, crater densities tend to be larger on the Mars side, anti-Mars side, tracking side, and leading side, in that order.

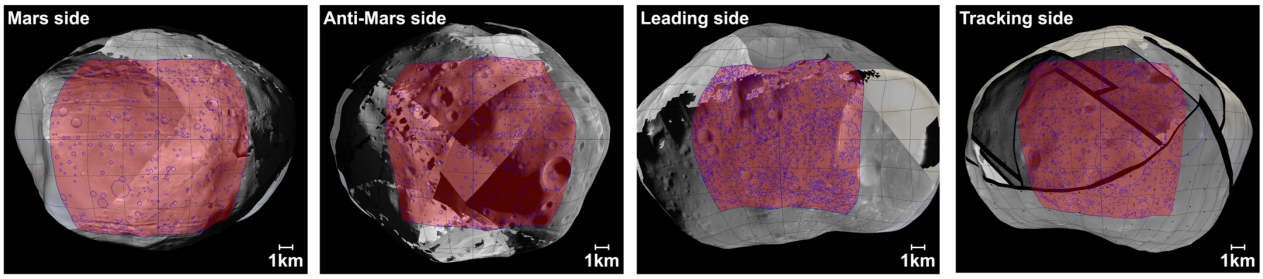

Figure 1. The 4 categories of Phobos (between 30°N and 30°S): Mars side (330°–360°W, 0°–30°W), anti-Mars side (150°–180°W, 180°–210°W), leading side (60°–90°W, 90°–120°W), and tracking side (240°–270°W, 270°–300°W). The circles represent the results of crater counting.

Table 1. The results of the crater counting. The results of the analysis are shown for the 8 regions between 30°N and 30°S every 30° longitude.

Region	**Mars side**		**Anti-Mars side**		**Leading side**		**Tracking side**	
Longitude	330°–360°W	0°–30°W	150°–180°W	180°–210°W	60°–90°W	90°–120°W	240°–270°W	270°–300°W
Area [km^2]	80.8	89.6	88.3	76.6	70.9	67.2	73.7	72.8
Max diameter [km]	2.9	1.2	2.3	1.31	0.81	3.2	3.7	1.97
Min diameter [km]	0.051	0.064	0.046	0.042	0.026	0.027	0.011	0.013
Power law index	2.58	2.61	2.98	2.23	3.04	2.57	1.76	1.68

Characteristic terrains. Comparison of the SFD for each area shows that the density of small craters in the Nearside, which includes the blue unit, is small. This indicates that there may have been some event that hid the smaller craters in this area. The formation of the blue unit may have been involved in this event.

Future work. We will determine whether the craters are clustered or random using the crater location information measured in this study.

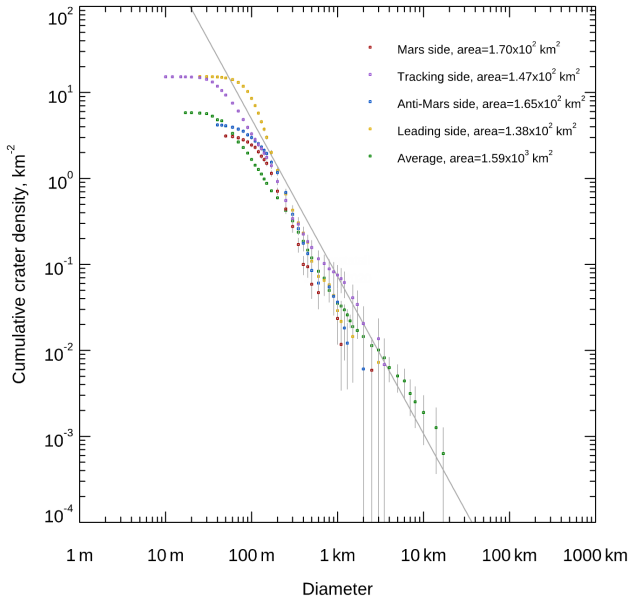

Figure 2. The cumulative crater size-frequency distribution. Each color represents the following areas. Red: Mars side, purple: tracking side, blue: anti-Mars side, yellow: leading side, green: average (PH9224GT).

Conclusion: In this study, crater analysis was performed in 8 regions of the Phobos low latitudes using a 3-D numerical shape model and high-resolution images. The cumulative crater size-frequency distribution was created based on the results of the crater analysis. Crater densities tend to be larger on the Mars side, anti-Mars side, tracking side, and leading side, in that order. The number density of small craters can be predicted from the data obtained in this study and can be used to select candidate landing areas for MMX mission. Further discussion of the characteristic geological features associated with crater formation is given as future works.

References: [1] Fraeman A. A. et al. (2014), *Icarus 229,* 196-205. [2] Murchie S. & Erard S (1996), *Icarus, 123*(1), 63-86. [3] Thomas P. et al. (1979), *Journal of Geophysical Research: Solid Earth 84.B14*, 8457-8477. [4] Veverka J. & Duxbury T. C. (1977), *Journal of Geophysical Research* 82.28, 4213-4223. [5] Basilevsky, A. T. (2014), *Planetary and Space Science 102*, 95-118. [6] Karachevtseva I. P. et al. (2014), *Planetary and Space Science, 102,* 74-85. [7] Ernst C. et al. (2018), *LPSC,* abstract #2083. [8] Michael G. G. & Neukum G. (2010), *Earth and Planetary Science Letters, 294*(3-4), 223-229. [9] Salamunicca G. et al. (2014), *Advances in Space Research, 53*(12), 1798-1809.